Chapter 5

The decaying phase of El Niño and Indian summer monsoon rainfall

Hyo-Seok Park[a], Won-il Lim[b] and Kyong-Hwan Seo[b]

[a]*Department of Ocean Science and Technology, Hanyang University, Ansan, South Korea*, [b] *Department of Atmospheric Sciences, Pusan National University, Busan, South Korea*

Abstract

Major winter El Niño events cause tropical Indian Ocean warming that persists into the following seasons. Previous studies have shown that Indian summer monsoon rainfall was above normal after major El Niño events due to anomalous warming over the North Indian Ocean (NIO). In this review, we revisit the delayed El Niño impact by analyzing the strongest events: 1982–1983, 1997–1998, and 2015–2016. During summers of 1983 and 1998, the influence of preceding winter El Niño event persisted into the summer via an anomalously warm NIO, with the latter in turn driving increasing rainfall over the Indian subcontinent. In 2016 summer, however, this warming was not followed by a significant increase in monsoon rainfall likely because NIO warming was weaker, whereas the warm sea surface temperature anomalies over the equatorial Indian Ocean persisted longer. These results highlight the importance of the Indian Ocean sea surface temperature pattern on monsoon variability.

Keywords: El Niño; North Indian Ocean; Indian summer rainfall; Precipitation; Sea surface temperature

5.1 Introduction

Intense research has been devoted to elucidate the mechanisms associated with the year-to-year fluctuations of South Asian summer monsoon, specifically rainfall over India. While Indian summer monsoon (ISM) rainfall is suppressed during the development of El Niño conditions in the tropical Pacific, rainfall over India increases during the summer following the winter peak of El Niño (Chowdary et al., 2017; Lau and Nath, 2012; Park et al., 2010; Shukla, 1995; Tao et al., 2016; Webster et al., 1998; Yang et al., 2007), which is referred to as the "delayed effect" (Park et al., 2010). One potential cause of this delayed effect is the transition to La Niña conditions after strong El Niño events (Chowdary et al., 2017; Shukla, 1995), but La Niña does not always follow El Niño events. On the other hand, the basin-wide tropical Indian Ocean warming that develops during, and persists after, El Niño events

Indian Summer Monsoon ENSO and Non-ENSO Teleconnections. https://doi.org/10.1016/B978-0-12-822402-1.00004-1

may contribute to enhanced ISM rainfall (Park et al., 2010; Terray et al., 2003).

Attribution of ISM rainfall variability to tropical Indian Ocean warming remains elusive. Indeed, tropical Indian Ocean warming after the mature phase of El Niño events has been regarded as a factor for suppressing the monsoon onset (Joseph et al., 1994; Lau and Nath, 2012), as persistent El Niño–induced off-equatorial South Indian Ocean warming may delay ISM onset by a week (Annamalai et al., 2005). Boreal spring warming of the southwest tropical Indian Ocean could generate North Indian Ocean (NIO) warming by inducing anomalous northerlies, which in turn suppress surface latent heat flux and thus establish a positive tendency in the ocean surface heat budget (Lau and Nath, 2012; Park et al., 2010). As the NIO warms, the thermodynamic regulation of surface latent heat flux (Park et al., 2010) begins to dominate over windspeed, increasing latent heat flux, and ultimately ISM rainfall (Park et al., 2010; Terray et al., 2003).

In the summer of 1983, following the 1982–1983 major winter El Niño, a notable NIO warming occurred, whereas the anomalously warm sea surface temperatures (SSTs) over the equatorial Indian Ocean somewhat dissipated. Although such an SST pattern may favor increased ISM rainfall (Chung and Ramanathan, 2006), this pattern does not occur with every El Niño event. In 2016, for example, anomalously high SSTs in the equatorial and the off-equatorial South Indian Ocean persisted throughout the summer (Chowdary et al., 2019b); the anomalous SST distribution in 2016 may have contributed to suppressing ISM rainfall. Furthermore, the atmospheric circulation pattern over the South Asian monsoon region during the post El Niño summers is not only affected by the Indian Ocean SST pattern but also by subtropical Northwest Pacific SST anomalies (e.g., Chowdary et al., 2017; Kosaka et al., 2013; Park et al., 2010; Xie et al., 2009).

In other words, the predictability of the peak-to-decaying phase El Niño subsequent summer-time ISM rainfall appears to be highly dependent on the details of the spatial pattern and temporal evolution of the Indo-Western Pacific SST anomalies. Likewise, the delayed effect is weakly supported by the statistical correlation on interannual time scales. The interannual correlation coefficient between the preceding winter Niño 3.4 index and ISM rainfall averaged from June to August is ~0.4, which is statistically weak (Park et al., 2010). Although it has been suggested that the relationship between decay phase El Niño conditions and ISM rainfall has strengthened recently (Chakravorty et al., 2016), the statistical relationship is still marginally significant.

In this chapter, we revisit the seasonal evolution of Indian Ocean SSTs and the accompanying impact on the ISM rainfall after three major El Niño events, 1982–1983 (82/83), 1997–1998 (97/98), and 2015–2016 (15/16). It has been previously reported that the El Niños of 1982–1983 and 1997–1998 caused off-equatorial South Indian Ocean warming in the spring and the subsequent northward progress of the warm anomalies that eventually led to the anom-

alously strong rainfall over the Indian subcontinent in August–September (Park et al., 2010). However, the northward progression of SST anomalies and the associated rainfall increase does not appear clearly in the spring and summer of 2016 (Chowdary et al., 2019b). Here, we revisit the delayed effect by adding the recent 2015–2016 El Niño event, which is one of the strongest events recorded in the last 145 years, comparable in magnitude to the 1997–1998 El Niño of the century (e.g., Huang et al., 2016; Jacox et al., 2016; Paek et al., 2017). We examine the Indian Ocean SST anomalies in the spring and summer of 2016 and the associated response of the ISM rainfall and compare with previous strong events, such as 1982–1983 and 1997–1998. Section 5.3.1 describes the spatial and temporal evolution of SST and low-level wind anomalies in the Indian Ocean following the three major El Niño events. In section 5.3.2, the ISM rainfall responses to the three major El Niño events are investigated in detail.

5.2 Methods and data used

To understand the dynamical processes associated with ISM precipitation during the decaying phase of El Niño, used monthly mean atmospheric reanalysis data. The atmospheric variables, including 10m zonal and meridional winds, vertically integrated moisture flux, and moisture flux convergence from the European Center for Medium-Range Weather Forecasts version 5 (ERA5) reanalysis hourly gridded dataset, have a horizontal resolution of 0.25° × 0.25° and cover January 1979 through December 2018 (Hersbach et al., 2020). To study the seasonal variability of SST, the Extended Reconstructed Sea Surface Temperature version 5 (ERSSTv5) dataset with a horizontal grid of 0.25° × 0.25° is employed for the period from January 1979 to December 2018 (Huang et al., 2017). To examine the Indo-Western Pacific precipitation anomalies, we used the Global Precipitation Climatology Project (GPCP) v2.3 monthly data, spanning January 1979 to December 2018. The GPCP v2.3 combines rain gauge observations and satellite precipitation and has a 2.5° × 2.5° horizontal resolution (Adler et al., 2018).

To identify the statistical relationship between El Niño and ISM rainfall, we analyzed the monthly El Niño and Indian summer monsoon rainfall indices. In addition to GPCP, we have used the Homogeneous Indian Monthly Rainfall Data Sets, which comprises monthly mean rainfall data spanning from 1987 to 2016 provided by the Indian Institute of Tropical Meteorology. We used Niño 3.4 index, which is calculated by averaging SST anomalies over the eastern Pacific from 5°S–5°N, 170°–120°W in the analysis. To identify the time-varying relationship between the preceding winter El Niño and the Indian summer monsoon rainfall index, 15-year running average between the preceding winter (Niño 3.4 index averaged from November to January) and All-ISM rainfall index (from June to September) is calculated, which is presented in

Fig. 5.1A. For example, the correlation coefficient in the year 2000 is calculated using the time period 1993–2007.

The climatological means are calculated using 40-year (1979–2018) monthly long-term means of the individual variable, including surface latent heat flux, 10m winds, vertically integrated moisture flux, and moisture flux convergence, SST, and precipitation. Because of the obvious increasing trend of SST, the seasonal-mean linear trends of SST at each grid are removed prior to calculating the anomalies.

5.3 Indian summer monsoon rainfall during El Niño decay

All ISM rainfall index over the entire monsoon season (June–September, hereafter JJAS) from 1979 to 2018 shows a large interannual variability (Fig. 5.1). Fig. 5.1A shows the 15-year moving window correlation between the preceding winter (November–January) El Niño, specifically the Niño 3.4 index averaged from November to January, and the JJAS ISM rainfall index. The correlation coefficient ranges from 0.3 to 0.5, which is statistically weak. The 39-year correlation from 1979/1980 to 2017/2018 between the preceding winter Niño and the ISM rainfall is 0.38, which explains approximately 15% of the interannual variance. As noted by Park et al. (2010), the ISM rainfalls were higher than normal following the two major winter El Niño events, 1982–1983 and 1997–1998 (Fig. 5.1B) and these above-normal rainfalls were particularly notable during the late monsoon season, August–September (Fig. 5.1C). However, the recent major El Niño event of 2015–2016 was not followed by above-normal monsoon rainfall in the summer of 2016 (Fig. 5.1B).

Although the delayed impact of the preceding winter El Niño on ISM rainfall is statistically weak, the NIO warming in the summer monsoon season is far more robust (Fig. 5.2). The lagged correlation between the preceding winter (November–January) Niño 3.4 index and the summer (JJAS average) SSTs from 1979 to 2018 shows a clear NIO warming (Fig. 5.2A), which is consistent with previous studies (Park et al., 2010). A majority of grid cells over the NIO shows statistically significant ($P < .05$) correlation coefficients, generally higher than 0.4, verifying the relatively robust impact of the preceding winter El Niño on the summer NIO SSTs. Unlike the NIO warming, precipitation responses are less robust. While the lagged correlations between the preceding winter Niño3.4 index and the summer precipitation are mostly positive over the NIO and neighboring Indian subcontinent, only a few grid cells exhibit statistically significant values (Fig. 5.2B). It is worth noting that the lower tropospheric wind anomalies are westward, implying weaker monsoonal westerlies (vectors in Fig. 5.2B), which suppress surface latent heat flux and thereby contributing to the summer NIO SST warming (Park et al., 2010; Lau and Nath., 2012).

While the lagged correlation maps present canonical patterns of summer SST and precipitation following the winter El Niño, the individual event

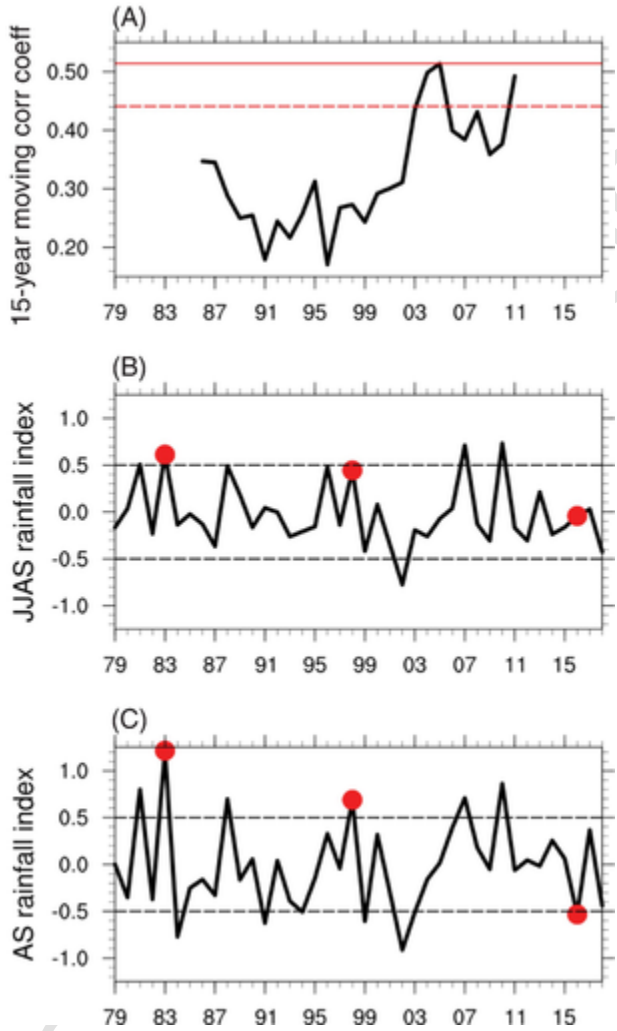

FIG. 5.1 (A) The 15-year running-window correlation between the preceding winter Niño 3.4 index and the standardized JJAS mean All-India summer monsoon rainfall index. Correlation coefficients above the red-solid line (*red-dotted line*) are statistically significant at 95% (90%) confidence interval. The 39-year correlation coefficient is 0.38. (B) Standardized June–September mean All-Indian summer monsoon rainfall index and the years with the three major winter El Niños before the summer monsoon season (*red dots*). (C) same as (A), except for late season (August–September; AS) Indian summer monsoon rainfall. In (B, C) dotted lines indicate ±0.5 standard deviations of monsoon rainfall.

shows a different SST pattern and a different precipitation response. Examining the SST responses to the individual El Niño event is necessary toward a better understanding of the delayed impact on ISM rainfall. In the next sec-

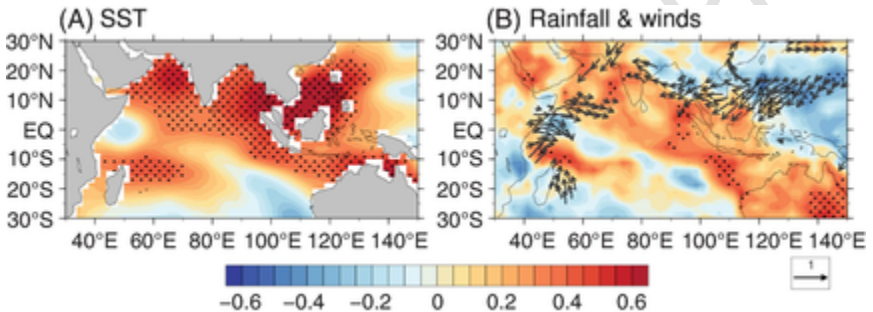

FIG. 5.2 Lagged correlations between the preceding winter (November–January) Niño 3.4 index and June–September mean (A) SST anomalies and (B) precipitation (shadings) with 850-hPa wind (vectors) anomalies. Statistically significant values ($P < .05$) are stippled. As for 850-hPa winds, only statistically significant values ($P < .05$) are presented. "*SST*, sea surface temperature."

tions, we examine the seasonal SST and precipitation anomalies for the major winter El Niño events, 1982–1983, 1998–1999, and 2015–2016, respectively.

5.3.1 Seasonal SST anomalies

The major winter El Niño events are robustly followed by basin-wide tropical Indian Ocean warming (Fig. 5.3A–C) and this El Niño induced remote tropical SST warming has been extensively investigated. Specifically, El Niño events warm the tropical Indian Ocean (20°S–20°N) by suppressing surface heat fluxes (Chiang and Lintner, 2005; Wu et al., 2008; Wu and Yeh, 2010) and by ocean dynamic processes (Du et al., 2009; Liu and Alexander, 2007; Xie et al., 2002; Chowdary and Gnanaseelan, 2007; Kakatkar et al. 2020). While all the three major El Niño events are followed by basin-wide tropical Indian Ocean warming, the detailed spatial structure and the seasonal evolution of SST anomalies for the three events contain some substantial differences.

In the following spring of all three major winter El Niño events, 1983, 1998, and 2016, warm SST anomalies develop in the equatorial and off-equatorial South Indian Ocean (Fig. 5.3A–C), which can be interpreted as a typical response to El Niño (Chen et al., 2019; Chowdary and Gnanaseelan, 2007; Chowdary et al., 2009; Lau and Nath, 2003; Xie et al., 2002). However, their seasonal progressions over the Indian Ocean contain similarities and differences. In the summer of 1983 and 1998, the equatorial and south equatorial warm Indian Ocean SST anomalies dissipated, whereas the warm NIO signal slightly strengthened (Fig. 5.3D and E). This seasonal progression of SSTs over the Indian Ocean, specifically the NIO warming in the summer being preceded by the equatorial Indian Ocean warming, can be clearly seen in Hovmöller plot (Fig. 5.4A and B). Here, the longitudinal range is averaged from 40°E to 90°E that covers the entire Western Indian Ocean including the Arabian Sea and the Bay of Bengal. As noted by Park et al. (2010), the SST anomalies averaged over the longitudinal sector of the Indian Ocean exhibit a northward progression of warm SST anomalies both in 1983 and 1998, although the zonal (east-west) SST anomalies were remarkably different each other: the maximum warm SST anomalies exist over the Western Pacific and South China Sea in the summer of 1998, whereas 1983 event has its maximum warm anomalies over the Arabian Sea (Fig. 5.3D and E).

In the summer of 2016, northward progression of warm SST anomalies over the Indian Ocean does not appear. The equatorial and the off-equatorial South Indian Ocean warming, which is a typical response to El Niño, appears (Fig. 5.3C) and the basin-wide Indian Ocean warming is stronger than those of 1983 and 1998. Unlike 1998, however, the warm SST anomalies over the NIO in the spring rapidly dissipated in the summer of 2016 (Fig. 5.3C and F). Therefore, the meridional gradient of SST anomalies over the Indian Ocean in the summer of 2016 is reversed, i.e., more warming in the south, which can

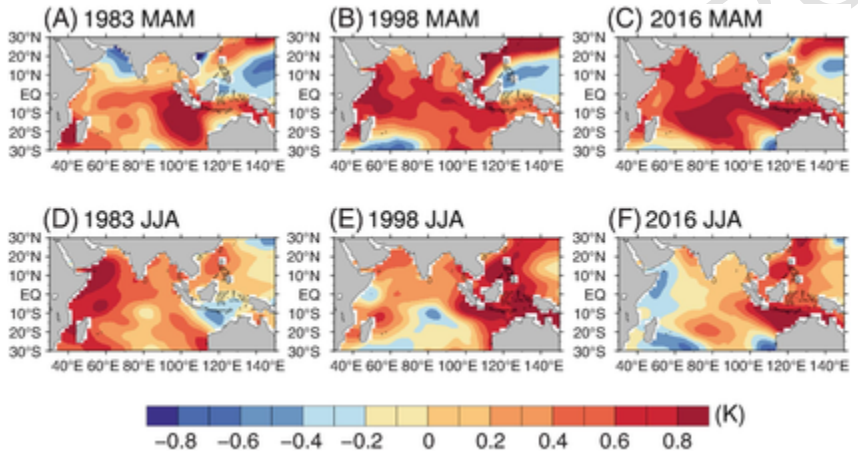

FIG. 5.3 Seasonal transitions of anomalous SSTs (K) during the (A–C) spring (March–May) and the (D–F) summer (June–August) after the three major winter El Niño events: (A, D) 1983, (B, E) 1998, and (C, F) 2016. "*SST*, sea surface temperature."

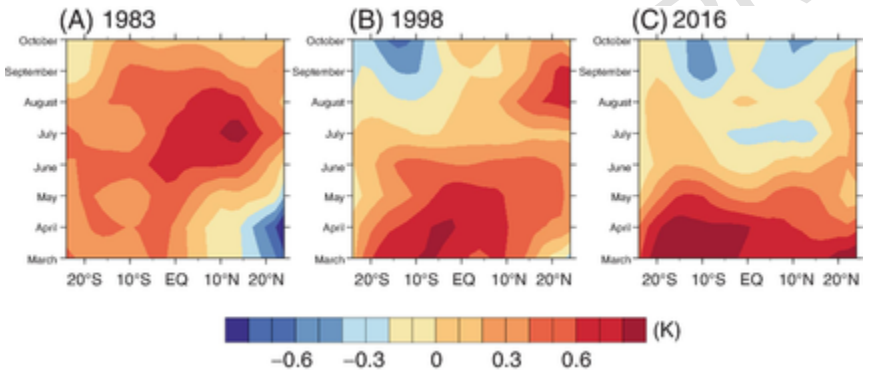

FIG. 5.4 Hovmöller diagram (40°–90°E longitudinal mean) of anomalous SST (K) following (A) 1982–1983, (B) 1997–1998 and (C) 2015–2016 major winter El Niño events. "*SST*, sea surface temperature."

weaken the ISM rainfall (Chung and Ramanathan, 2006). The Hovmöller plot averaged over the Indian Ocean clearly shows that the anomalously warm NIO relative to the equatorial Indian Ocean in the summer of 1983 and in the late summer (August–September) of 1998 (Fig. 5.4A and B) does not appear in 2016 (Fig. 5.4C). Because the warm SST anomalies over the off-equatorial South Indian Ocean persist into the summer of 2016 (Figs 5.3F and 5.4C), the meridional SST gradient effect on the ISM rainfall rather weakens. Furthermore, it is worth noting that the warm Indian Ocean SST anomalies in the spring of 2016 are wider and stronger than those of 1983 and 1998. More pronounced tropical Indian Ocean warming is observed in the spring and these SST anomalies are spatially uniform, including the Arabian Sea SST warming, which is up to ~0.7 K (Fig. 5.3C). The long-term background warming in 2015–2016 El Niño, which is associated with unusually warm conditions in 2014 (Santoso et al., 2017) is likely to be a factor for the stronger Indian Ocean warming than previous major El Niño events. In summary, the Indian Ocean warming in the spring of 2016 is generally stronger than that of previous major El Niño events, but this strong warming is not followed by the NIO warming in the summer.

5.3.2 Monsoonal winds and moisture transport

The surface wind weakening, specifically the weakening of westerlies over NIO and the associated surface latent heat suppression in the spring and summer, has been suggested as a principal driver of the NIO warming (Lau and Nath, 2012; Park et al., 2010). In the summer of 1983 and 1998, the surface wind anomalies over NIO are easterlies, both in the Bay of Bengal and Arabian Sea (Fig. 5.5A and B). These easterly anomalies are not limited to NIO but extend to the subtropical Western North Pacific (10°–25°N), where anomalous anticyclonic winds develop (Xie et al., 2009). The internal feedback between the anomalously warm NIO and the anticyclonic winds over the subtropical North Pacific, so-called the Philippine Sea anticyclones, has been well established (Annamalai et al., 2005; Kosaka et al., 2013; Stuecker et al., 2015; Watanabe and Jin, 2003; Xie et al., 2009). This interbasin feedback is referred to as the Indo-Western Pacific ocean capacitor mode (Xie et al., 2016). The warmer NIO generates eastward propagating atmospheric Kelvin waves, which would maintain the Philippine Sea anticyclones (Xie et al., 2009). Conversely, the weakening of convection over the subtropical western North Pacific (10°–25°N) generates a cold Rossby wave that can suppress precipitation westward to the Bay of Bengal (Kosaka et al., 2013; Srinivas et al. 2018). In the summer of 1983 and 1998, the development of surface anticyclones over the subtropical Western North Pacific and the associated decrease in precipitation over South China Sea and the Bay of Bengal appear (Fig. 5.5A and B).

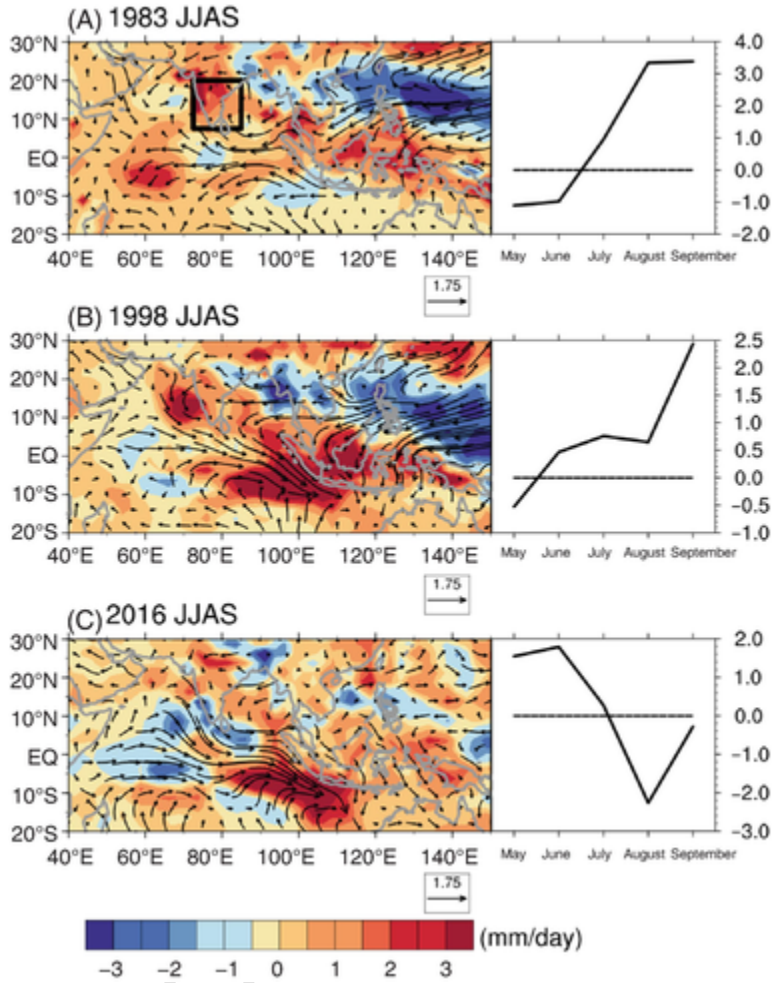

FIG. 5.5 June–September mean precipitation anomalies (shadings: mm/day) and surface wind anomalies (vectors: m/s) in (A) 1983, (B) 1998, and (C) 2016. Right-hand side panels are monthly precipitation anomalies from May to September averaged over the black square in (A) (8°–20°N, 70°–85°E).

Despite the weakening of monsoonal westerlies over NIO, precipitation is above normal over the Indian subcontinent in the summer of 1983 and 1998 (right panel figures in Fig. 5.5A and B). The paradox of the increased monsoon rainfall associated with the weaker monsoon circulation has been previously addressed by a few general circulation model (GCM) studies under global warming scenarios (Kitoh et al., 1997; Stowasser et al., 2009) and by a more realistic El Niño case with atmospheric GCM coupled to a slab

ocean model (Park et al., 2010). As noted in Park et al. (2010), the monsoonal low-level wind strength does not necessarily represent the monsoonal convective strength, but moist processes, such as moisture flux convergence associated with the warmer NIO can compensate the wind effect. Indeed, Fig. 5.6 shows that the vertically integrated moisture flux anomalies are eastward over the subcontinent of India, Bay of Bengal, and the South China Sea (vectors in Fig. 5.6), which are generally consistent with the lower-tropospheric wind anomalies (vectors in Fig 5.5). However, the weakening of monsoonal winds and the associated moisture fluxes are accompanied by strengthened

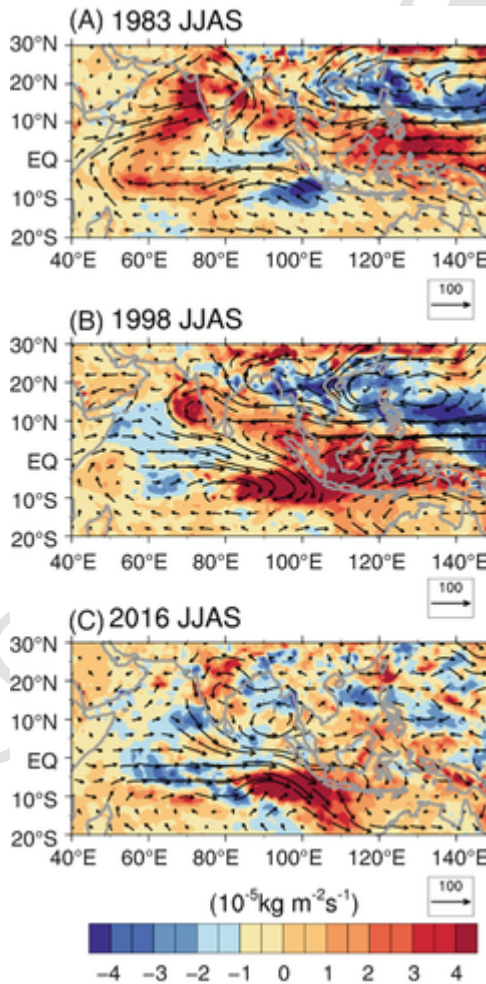

FIG. 5.6 June–September mean composites of the anomalous moisture flux (vectors: (kg/m/s) and moisture flux convergence (shadings: kg/m^2/s) in (A) 1983, (B) 1998, and (C) 2016.

moisture flux convergence over subcontinent of India (shadings in Fig. 5.6), which may explain the paradox of increased monsoon rainfall with the weaker monsoon circulation. Recent studies suggest that northwestward propagating Rossby waves induced by anomalous heating over the Maritime continent can enhance the rainfall over southern peninsular India during decay phase of El Niño years (Chowdary et al., 2019a; Srinivas et al., 2018), which can partly explain the paradox.

The weakening of NIO-region surface wind speeds during the early phase of the monsoon followed by a later rebound toward climatological values during 1983 and 1998, especially in September (Park et al., 2010), contributes to the notable increase in monsoon rainfall (right panel figures in Fig. 5.5A and B). In the summer of 2016, however, the basin-wide weakening of South Asian monsoon circulation that is also dynamically tied to the anomalous Philippine Sea anticyclone does not appear (Fig. 5.5C). The absence of the systematic weakening of NIO-region surface wind speed might explain the relatively weak NIO warming in the summer of 2016 (Figs 5.3F and 5.4C). Because the NIO warming signal is weak, whereas the anomalously high SSTs persist over the off-equatorial South Indian Ocean, all ISM rainfall index is close to normal in 2016 (Fig. 5.1). The subseasonal precipitation anomalies in 2016 are almost opposite to those of previous El Niño events: while precipitation is above-normal in the early monsoon season (May–June), the late monsoon season (August–September) precipitation is lower than average (right panel figure in Fig. 5.5C). The absence of the anomalous Philippine Sea anticyclone in the summer of 2016 suggests that the development of the Philippine Sea anticyclone, which contributes to weakening the low-level monsoonal winds, which in turn warms the NIO, is probably an important factor for increasing the moisture flux convergence and the associated ISM rainfall after major winter El Niño events. This analogy is supported by recent GCM experiments (Chowdary et al., 2019a; Srinivas et al., 2018), which verified the close connection between the anomalous Philippine Sea anticyclone and the increased ISM rainfall after major winter El Niño events.

5.4 Summary and discussion

In this review article, we have revisited the so-called delayed effect of major winter El Niño events on subsequent Indian Ocean SST warming and the ISM rainfall increases by including the 2015–16 El Niño event, an event of similar magnitude to prior events (1983 and 1998) for which a delayed effect is inferred. In the earlier events, the influence of preceding winter El Niño event persists into the ISM season via an anomalously warm NIO, with the latter in turn driving increasing rainfall over the NIO and neighboring Indian subcontinent. During both 1983 and 1998, the occurrence of weakening of low-level monsoonal winds and the suppression of surface latent heat flux during the late spring and summer is reported. Moreover, the presence of an anomalous

Philippine Sea anticyclone is consistent with the weakening of low-level winds over NIO. Relaxation of the winds, through latent heat flux suppression, is in turn consistent with NIO warming. In 2016, however, the basin-wide NIO warming did not follow the basin-wide spring tropical Indian Ocean warming, possibly because a strong Philippine sea surface anticyclone failed to develop (Chowdary et al., 2019b). As suggested by GCM experiments (Chowdary et al., 2019a; Srinivas et al., 2018), the feedback between the NIO and the Philippine Sea surface anticyclones is a key to the NIO warming and increasing the ISM rainfall. In 1983 and 1998, the warm El Niño conditions in the eastern Pacific slowly decayed and persisted into the spring season, which has been suggested as a key driver of the NIO warming in the summer (Park et al., 2010).

It is noted that the Niño 3 index representing the eastern equatorial Pacific SST anomaly was more positive in the spring (April–May) of 1998 than that of 2016, although a transition into La Niña condition was suppressed in the summer of 2016 (Kakatkar et al., 2018). It is likely that the early decay of the anomalously warm SSTs in the Eastern Pacific in the spring of 2016 led to the weakening of the Philippine Sea surface anticyclones. Predicting the summer basin-wide tropical Indian Ocean/NIO warming patterns during El Niño decay would be useful for ISM rainfall prediction. Further numerical modeling studies on the decaying phase of El Niño, such as the persistence of the warm eastern Pacific SST in the spring, are needed to better understand the delayed impact of winter El Niño on the monsoon circulation strength and ISM rainfall.

Acknowledgments

We would like to thank Benjamin Lintner for helpful comments and for proofing the manuscript. H.-S.P. is supported by the National Research Foundation of Korea (NRF) no. 2020R1A2C2010025.

References

Adler, R., Sapiano, M., Huffman, G., Wang, J.-J., Gu, G., Bolvin, D., et al., 2018. The Global Precipitation Climatology Project (GPCP) monthly analysis (New Version 2.3) and a review of 2017 global precipitation. Atmosphere (Basel) 9, 138. doi:10.3390/atmos9040138.

Annamalai, H., Liu, P., Xie, S.P., 2005. Southwest Indian Ocean SST variability: its local effect and remote influence on Asian monsoons. J. Clim. 18, 4150–4167. doi:10.1175/JCLI3533.1.

Chakravorty, S., Gnanaseelan, C., Pillai, P.A., 2016. Combined influence of remote and local SST forcing on Indian summer monsoon rainfall variability. Clim. Dyn. 47, 2817–2831. doi:10.1007/s00382-016-2999-5.

Chen, Z., Du, Y., Wen, Z., Wu, R., Xie, S.P., 2019. Evolution of south tropical Indian ocean warming and the climatic impacts following strong el niño events. J. Clim. 32, 7329–7347. doi:10.1175/JCLI-D-18-0704.1.

Chiang, J.C.H., Lintner, B.R., 2005. Mechanisms of remote tropical surface warming

during El Niño. J. Clim. 18, 4130–4149. doi:10.1175/JCLI3529.1.
Chowdary, J.S., Gnanaseelan, C., 2007. Basin-wide warming of the Indian Ocean during El Niño and Indian Ocean dipole years. Int. J. Climatol. 27, 1421–1438. doi:10.1002/joc.1482.
Chowdary, J.S., Gnanaseelan, C., Xie, S.P., 2009. Westward propagation of barrier layer formation in the 2006–07 Rossby wave event over the tropical southwest Indian Ocean. Geophys. Res. Lett. 36 (4). doi:10.1029/2008GL036642.
Chowdary, J.S., Harsha, H.S., Gnanaseelan, C., Srinivas, G., Parekh, A., Pillai, P., et al., 2017. Indian summer monsoon rainfall variability in response to differences in the decay phase of El Niño. Clim. Dyn. 48, 2707–2727. doi:10.1007/s00382-016-3233-1.
Chowdary, J.S., Patekar, D., Srinivas, G., Gnanaseelan, C., Parekh, A., 2019a. Impact of the Indo-Western Pacific Ocean Capacitor mode on South Asian summer monsoon rainfall. Clim. Dyn. 53, 2327–2338. doi:10.1007/s00382-019-04850-w.
Chowdary, J.S., Srinivas, G., Du, Y., Gopinath, K., Gnanaseelan, C., Parekh, A., et al., 2019b. Month-to-month variability of Indian summer monsoon rainfall in 2016: role of the Indo-Pacific climatic conditions. Clim. Dyn. 52, 1157–1171. doi:10.1007/s00382-018-4185-4.
Chung, C.E., Ramanathan, V., 2006. Weakening of north Indian SST gradients and the monsoon rainfall in India and the Sahel. J. Clim. 19, 2036–2045. doi:10.1175/JCLI3820.1.
Du, Y., Xie, S.P., Huang, G., Hu, K., 2009. Role of air-sea interaction in the long persistence of El Niño-induced north Indian Ocean warming. J. Clim. 22, 2023–2038. doi:10.1175/2008JCLI2590.1.
Hersbach, H., Bell, B., Berrisford, P., Hirahara, S., Horányi, A., Muñoz-Sabater, J., et al., 2020. The ERA5 global reanalysis. Q. J. R. Meteorol. Soc. 146, 1999–2049. doi:10.1002/qj.3803.
Huang, B., L'Heureux, M., Hu, Z.Z., Zhang, H.M., 2016. Ranking the strongest ENSO events while incorporating SST uncertainty. Geophys. Res. Lett. 43, 9165–9172. doi:10.1002/2016GL070888.
Huang, B., Thorne, P.W., Banzon, V.F., Boyer, T., Chepurin, G., Lawrimore, J.H., et al., 2017. Extended reconstructed Sea surface temperature, Version 5 (ERSSTv5): upgrades, validations, and intercomparisons. J. Clim. 30, 8179–8205. doi:10.1175/JCLI-D-16-0836.1.
Jacox, M.G., Hazen, E.L., Zaba, K.D., Rudnick, D.L., Edwards, C.A., Moore, A.M., Bograd, S.J., 2016. Impacts of the 2015–2016 El Niño on the California Current System: Early assessment and comparison to past events. Geophys. Res. Lett. 43, 7072–7080. doi:10.1002/2016GL069716.
Joseph, P.V., Eischeid, J.K., Pyle, R.J., 1994. Interannual variability of the onset of the Indian summer monsoon and its association with atmospheric features, El Nino, and sea surface temperature anomalies. J. Clim. 7, 81–105 (1994)007<0081:IVOTOO>2.0.CO;2 doi:10.1175/1520-0442.
Kakatkar, R., Gnanaseelan, C., Chowdary, J.S., 2020. Asymmetry in the tropical Indian Ocean subsurface temperature variability. Dyn. of Atmos. Ocean. 90, 101142. doi:10.1016/j.dynatmoce.2020.101142.
Kakatkar, R., Gnanaseelan, C., Deepa, J.S., Chowdary, J.S., Parekh, A., 2018. Role of ocean-atmosphere interactions in modulating the 2016 La Niña like pattern over the tropical Pacific. Dyn. Atmos. Ocean. 83, 100–110. doi:10.1016/j.dynatmoce.2018.07.003.
Kitoh, A., Yukimoto, S., Noda, A., Motoi, T., 1997. Simulated changes in the Asian summer monsoon at times of increased atmospheric CO_2. J. Meteorol. Soc. Japan. Ser. II 75, 1019–1031. doi:10.2151/jmsj1965.75.6_1019.
Kosaka, Y., Xie, S.P., Lau, N.C., Vecchi, G.A., 2013. Origin of seasonal predictability for summer climate over the Northwestern Pacific. Proc. Natl. Acad. Sci. U. S. A.

110, 7574–7579. doi:10.1073/pnas.1215582110.
Lau, N.C., Nath, M.J., 2012. A Model study of the air-sea interaction associated with the climatological aspects and interannual variability of the South Asian summer monsoon development. J. Clim. 25, 839–857. doi:10.1175/JCLI-D-11-00035.1.
Lau, N.C., Nath, M.J., 2003. Atmosphere-ocean variations in the Indo-Pacific sector during ENSO episodes. J. Clim. 16, 3–20 (2003)016<0003:AOVITI>2.0.CO;2 doi:10.1175/1520-0442.
Liu, Z., Alexander, M., 2007. Atmospheric bridge, oceanic tunnel, and global climatic teleconnections. Rev. Geophys.. doi:10.1029/2005RG000172.
Paek, H., Yu, J.Y., Qian, C., 2017. Why were the 2015/2016 and 1997/1998 extreme El Niños different? Geophys. Res. Lett. 44, 1848–1856. doi:10.1002/2016GL071515.
Park, H.S., Chiang, J.C.H., Lintner, B.R., Zhang, G.J., 2010. The delayed effect of major El Niño events on Indian monsoon rainfall. J. Clim. 23, 932–946. doi:10.1175/2009JCLI2916.1.
Santoso, A., Mcphaden, M.J., Cai, W., 2017. The defining characteristics of ENSO extremes and the strong 2015/2016 El Niño. Rev. Geophys. doi:10.1002/2017RG000560.
Shukla, J., 1995. Predictability of the tropical atmosphere, the tropical oceans and TOGA. In: Proc. Int. Sci. Conf. Trop. Ocean Glob. Atmos. Program. WCRP-91, WMO/TD 717, 2. Melbourne, pp. 725–730.
Srinivas, G., Chowdary, J.S., Kosaka, Y., Gnanaseelan, C., Parekh, A., Prasad, K.V.S.R., 2018. Influence of the Pacific-Japan pattern on Indian summer monsoon rainfall. J. Clim. 31, 3943–3958. doi:10.1175/JCLI-D-17-0408.1.
Stowasser, M., Annamalai, H., Hafner, J., 2009. Response of the South Asian summer monsoon to global warming: mean and synoptic systems. J. Clim. 22, 1014–1036. doi:10.1175/2008JCLI2218.1.
Stuecker, M.F., Jin, F.F., Timmermann, A., Mcgregor, S., 2015. Combination mode dynamics of the anomalous northwest pacific anticyclone. J. Clim. 28, 1093–1111. doi:10.1175/JCLI-D-14-00225.1.
Tao, W., Huang, G., Hu, K., Gong, H., Wen, G., Liu, L., 2016. A study of biases in simulation of the Indian Ocean basin mode and its capacitor effect in CMIP3/CMIP5 models. Clim. Dyn. 46, 205–226. doi:10.1007/s00382-015-2579-0.
Terray, P., Delecluse, P., Labattu, S., Terray, L., 2003. Sea surface temperature associations with the late Indian summer monsoon. Clim. Dyn. 21, 593–618. doi:10.1007/s00382-003-0354-0.
Watanabe, M., Jin, F.F., 2003. A moist linear baroclinic model: coupled dynamical-convective response to El Niño. J. Clim. 16, 1121–1139 (2003)16<1121:AMLBMC>2.0.CO;2 doi:10.1175/1520-0442.
Webster, P.J., Magaña, V.O., Palmer, T.N., Shukla, J., Tomas, R.A., Yanai, M., et al., 1998. Monsoons: processes, predictability, and the prospects for prediction. J. Geophys. Res. Ocean. 103, 14451–14510. doi:10.1029/97jc02719.
Wu, R., Kirtman, B.P., Krishnamurthy, V., 2008. An asymmetric mode of tropical Indian Ocean rainfall variability in boreal spring. J. Geophys. Res. Atmos. 113 n/a-n/a doi:10.1029/2007JD009316.
Wu, R., Yeh, S.-W., 2010. A further study of the tropical Indian Ocean asymmetric mode in boreal spring. J. Geophys. Res. 115, D08101. doi:10.1029/2009JD012999.
Xie, S.P., Annamalai, H., Schott, F.A., McCreary, J.P., 2002. Structure and mechanisms of South Indian Ocean climate variability. J. Clim. 15, 864–878 (2002)015<0864:SAMOSI>2.0.CO;2 doi:10.1175/1520-0442.
Xie, S.P., Hu, K., Hafner, J., Tokinaga, H., Du, Y., Huang, G., et al., 2009. Indian Ocean capacitor effect on Indo-Western pacific climate during the summer following El Niño. J. Clim. 22, 730–747. doi:10.1175/2008JCLI2544.1.
Xie, S.P., Kosaka, Y., Du, Y., Hu, K., Chowdary, J.S., Huang, G., 2016. Indo-western Pacific ocean capacitor and coherent climate anomalies in post-ENSO summer: a

review. Adv. Atmos. Sci. 33, 411–432. doi:10.1007/s00376-015-5192-6.
Yang, J., Liu, Q., Xie, S.-P., Liu, Z., Wu, L., 2007. Impact of the Indian Ocean SST basin mode on the Asian summer monsoon. Geophys. Res. Lett. 34, L02708. doi:10.1029/2006GL028571.